

# Squint Spotlight SAR Raw Signal Simulation in the Frequency Domain Using Optical Principles

Yu Wang, *Member, IEEE*, Zhimin Zhang, and Yunkai Deng

**Abstract**—Synthetic aperture radar (SAR) distributed target scene raw signal simulation is an important tool for the study and test of SAR systems and processing algorithms, mission planning, and inversion algorithm design. In this paper, the squint spotlight SAR scene model is evaluated to achieve spotlight SAR raw signals in the 2-D frequency domain and the precision of the model is analyzed. It is known that the range migration phenomenon in the time domain is explained as the coupling between the range and azimuth in the 2-D frequency domain. To realize the coupling relation in the 2-D frequency, interpolation may be needed. However, interpolation is a time-consuming manipulation. For efficiency, some signal processing methods are employed to couple the range and azimuth frequencies. Those tricks are derived from some optical principles, which give us some novel thoughts. Therefore, the efficiency of the simulator is highly improved, which facilitates its application to the verification and test of the real-time processor.

**Index Terms**—Chirp Fourier transform, distributed target scene, fast Fourier transform (FFT), synthetic aperture radar (SAR).

## I. INTRODUCTION

**S**YNTHETIC aperture radar (SAR), which is used on mobile platforms such as airborne or spaceborne platforms, is an active imaging method based on microwaves. SAR is a coherent imaging sensor, and its all-weather day and night imaging capabilities coupled with the achievable high resolutions make it a fundamental instrument for Earth and other planet observations [1]. A SAR can be operated in a number of different ways, such as stripmap, scan, and spotlight. The resolution of the stripmap mode can be improved by increasing the angular extent of the illumination on the area of interest. The improvement of resolution given by the spotlight mode is in the along-track (azimuth) direction. This can be done by steering the beam overall acquisition time to illuminate the same area (a spot on the ground). The available synthetic antenna length can be increased with respect to the stripmap mode, thus improving azimuth resolution. This gain is traded off by the loss of coverage due to the illumination of a limited area along the sensor flight path [1].

With the further development of the SAR technology, some new SAR sensors are being developed. To test the SAR system and new signal processing algorithms, the SAR raw data simulator is desirable. Methods about SAR raw signal simulations are particularly described in [2]–[4]. Such a simulator would be really useful only if it meets some stringent requirements: it must account for both SAR system and scene characteristics; it must be able to deal with extended scenes and not just with limited scattering points; finally, the simulator can be implemented by hardware easily [5], [6]. The efficient simulation method of spotlight SAR is discussed in [5], which uses a perfect trick to overcome the key problem (i.e., the spotlight SAR system transfer function depends on the azimuth coordinate of ground point [1]). However, the method mainly concentrates on the broadside mode, and it does not give a detailed discussion about how to efficiently achieve the coupling relation between the range and azimuth, which is an essential characteristic of SAR signals.

In this paper, a squint spotlight SAR model is described. Moreover, the relative phase error arising from the nonlinear phase function approximation in the squint spotlight mode is analyzed and illustrated to show the accuracy of the squint spotlight SAR signal model. In order to precisely actualize the range migration phenomenon, a high-order interpolation kernel is required. However, it is time-consuming. Fortunately, we use some optical principles to deduce some signal processing algorithms in the 2-D frequency domain to overcome the challenging problem without using interpolation manipulation. Such methods can be regarded as an inversion problem of signal processing algorithms presented in [7], [8], and Bluestein's formula, but we deduce the methods from some novel perspectives, which come from simple optical theories. These algorithms, which only require complex multiplications and fast Fourier transforms (FFTs), are inherently phase preserving and suitable for the characteristics of squint spotlight SAR raw signals. What is particularly emphasized is that our model assumes a straight-line flight path. Moreover, in the process of computation reflectivity, transmitting and receiving polarization, incidence angles, electromagnetic parameters, and ground ranges to slant projections are beyond the scope of this paper and can be found in [2]–[4].

This paper is organized as follows. In Section II, a precise squint spotlight SAR signal model is evaluated in both space and frequency domain and its accuracy is analyzed. In Section III, we display how to obtain the 2-D coupling relation between range and azimuth through some optical principles. In Section IV, some simulation results are shown. Finally, some conclusions are reported in Section V.

Manuscript received September 7, 2006; revised January 9, 2008.

Y. Wang is with the Graduate University of Chinese Academy of Sciences, Beijing 100039, China (e-mail: robert.wy@gmail.com).

Z. Zhang and Y. Deng are with the Institute of Electronics, Chinese Academy of Sciences, Beijing 100080, China.

Color versions of one or more of the figures in this paper are available online at <http://ieeexplore.ieee.org>.

Digital Object Identifier 10.1109/TGRS.2008.917496

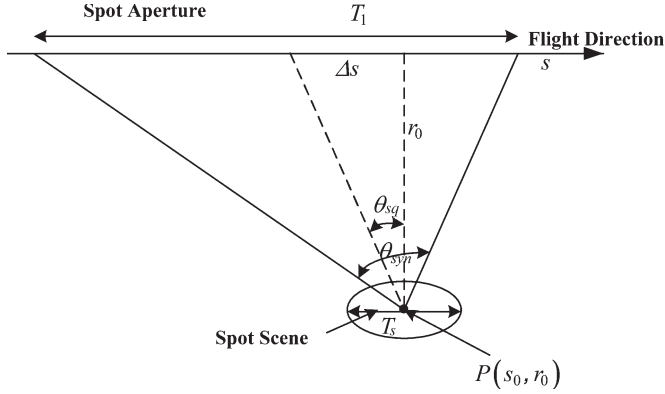


Fig. 1. Basic squint spotlight SAR geometry. The sensor moves along a straight flight direction in the azimuth. During the time of spotlight aperture, the beam is constantly pointed to the center of the scene. The antenna steering causes a longer spotlight aperture  $T_1$  and the shorter SAR scene aperture  $T_s$ . The squint angle is denoted by  $\theta_{sq}$ .

## II. SQUINT SPOTLIGHT SIGNAL MODEL AND SIMULATION PROCEDURE OF RAW SIGNAL

In this section, according to the squint spotlight SAR geometry shown in Fig. 1, we will show the model of the squint spotlight SAR signal. In the case of a straight flight, forward squint and down-converted with no dechirping on the receiver, a spotlight SAR echo signal located in  $(s_0, r_0)$  can be described as follows [9]:

$$rt(s-s_0, t, r_0) = \sigma(s_0, r_0) \exp\left(-j\frac{4\pi}{\lambda}R\right) \times \exp\left[j\pi K_r \left(t - \frac{2R}{c}\right)^2\right] \text{rect}\left[\frac{t-2R/c}{\tau}\right] \times \text{rect}\left[\frac{s+\Delta s}{T_1}\right] \text{rect}\left[\frac{s_0}{T_s}\right] \quad (1)$$

where

$$R = \sqrt{r_0^2 + v^2(s-s_0)^2} \quad (2)$$

$$T_1 = \frac{2r_0 tg(\theta_{syn}/2)}{v \cos^2(\theta_{sq}) [1 - tg^2(\theta_{syn}/2) tg^2(\theta_{sq})]} \quad (3)$$

$$\Delta s = r_0 tg(\theta_{sq})/v. \quad (4)$$

In (1)–(4),  $\lambda$  and  $c$  are the wavelength and speed of light, respectively,  $t$  and  $s$  are the range and azimuth time, respectively,  $(s_0, r_0)$  is the position of the azimuth time and slant-range domain of points in the illuminated scene,  $\sigma(s_0, r_0)$  is the scattering coefficient of the point target at position  $(s_0, r_0)$ ,  $v$  represents the platform's velocity,  $T_1$  and  $\theta_{syn}$  are the duration of full spotlight aperture and the synthetic aperture angle for the target at position  $(s_0, r_0)$ , respectively,  $T_s$  is the width of spotlight scene in the azimuth, and  $K_r$  and  $\tau$  are the chirp rate and pulse duration time of the transmitted signal, respectively.  $R$  is defined as the instantaneous range between the point target at position  $(s_0, r_0)$  and the antenna phase center,  $\text{rect}[(s+\Delta s)/T_1]$  accounts for the flight duration time during which data are received (see Fig. 1), and  $\Delta s$  is the offset of zero

Doppler time with respect to the scene center crossing time; if  $\Delta s = 0$ , our model becomes broadside;  $\text{rect}[s_0/T_s]$  is the simplified expression of the two-way antenna pattern, which is independent of the variable  $s$  because of the antenna steering operation.

The point-target signal must be integrated via all of the illuminated targets to obtain spotlight SAR raw signals in the whole scene

$$h_{spot}(s, t) = \iint_{\Sigma} rt(s-s_0, t, r_0) ds_0 dr_0. \quad (5)$$

In (5),  $\Sigma$  is expressed as the whole scene. Because the Doppler frequency is derived from relative motion between radar and targets,  $\text{rect}[(s+\Delta s)/T_1]$  in (1) causes the dependence of the transfer function on the azimuth coordinate of the ground point. It can be more clearly demonstrated if  $\text{rect}[(s+\Delta s)/T_1]$  is expressed as  $\text{rect}[(s-s_0) + (\Delta s + s_0)]/T_1]$ . To overcome the limitation of the dependence on the target azimuth coordinate, we add a function  $\text{rect}[(s-s_0 + \Delta s)/(T_1 + T_s)]$  into (1). The inclusion of the function does not alter the value of (1) because it is equal to one if both  $\text{rect}[(s+\Delta s)/T_1]$  and  $\text{rect}[s_0/T_s]$  are not null. This perfect trick is presented in [5]. Therefore, we have the following:

$$rt(s-s_0, t, r_0) = rt(s-s_0, t, r_0) \text{rect}\left[\frac{s-s_0+\Delta s}{T_1+T_s}\right]. \quad (6)$$

Then, the term  $\text{rect}[(s+\Delta s)/T_1]$  can be shifted out of the integration, and (6) can be rewritten as follows:

$$h_{spot}(s, t) = \text{rect}\left[\frac{s+\Delta s}{T_1}\right] \bar{h}_{spot}(s, t) \quad (7)$$

with

$$\bar{h}_{spot}(s, t) = \iint_{\Sigma} \sigma(s_0, r_0) \exp\left(-j\frac{4\pi}{\lambda}R\right) \times \exp\left[j\pi K_r \left(t - \frac{2R}{c}\right)^2\right] \cdot \text{rect}\left[\frac{t-2R/c}{\tau}\right] \times \text{rect}\left[\frac{s-s_0+\Delta s}{T_1+T_s}\right] \text{rect}\left[\frac{s_0}{T_s}\right] ds_0 dr_0. \quad (8)$$

The key to efficiently obtain the spotlight SAR raw signal is the calculation of the function  $\bar{h}_{spot}(s, t)$ . On the face of it, we may compute it via a 2-D superposition integral. However, superposition integral in the time domain is costly. However, when we consider it in detail, we can indirectly evaluate it in frequency domain via 2-D FFT. We transform (8) into a 2-D frequency domain and obtain

$$\bar{H}_{spot}(f_a, f) = \iint \bar{h}_{spot}(s, t) \times \exp(-j2\pi f_a s) \exp(-j2\pi f t) ds dt \quad (9)$$

where  $f$  and  $f_a$  are the range and azimuth frequency variables, respectively. In (9), we exchange the order of the integral and

have

$$\overline{H}_{\text{spot}}(f_a, f) = \iint_{\Sigma} \text{RF}(f_a, f; s_0, r_0) ds_0 dr_0. \quad (10)$$

Using the stationary phase theory, we can express the 2-D spectrum of point target as follows:

$$\begin{aligned} \overline{H}_{\text{spot}}(f_a, f) &= \text{RF}(f_a, f; s_0, r_0) \\ &= \mathbb{C} \sqrt{r_0} \exp[-j2\pi\Psi(f_a, f)] \text{rect}\left[\frac{s_0}{T_s}\right] \\ &\quad \times \text{rect}\left[\frac{f_a - f_{\text{Dc}}}{(1+T_1/T_s)B_a \cos\theta_{\text{sq}}}\right] \text{rect}\left[\frac{f}{B_d}\right] \\ &\quad \times \iint_{\Sigma} \text{RF}(f_a, f; s_0, r_0) ds_0 dr_0 \end{aligned} \quad (11)$$

$$\Psi_a(f_a, f) = \frac{f^2}{2K_r} + \frac{2r_0}{\lambda} \sqrt{\left(1 + \varepsilon \frac{f}{B_d}\right)^2 - \left(\frac{\lambda f_a}{2v}\right)^2} + f_a s_0 \quad (12)$$

$$\mathbb{C} = \sqrt{\frac{\lambda}{2v^2}} \frac{\left(1 + \varepsilon \frac{f}{B_d}\right)}{\left[\left(1 + \varepsilon \frac{f}{B_d}\right)^2 - \left(\frac{\lambda f_a}{2v}\right)^2\right]^{\frac{3}{4}}} \exp\left(-j\frac{\pi}{4}\right) \quad (13)$$

where  $f_{\text{Dc}} = 2v \sin\theta_{\text{sq}}/\lambda$  is the Doppler-centroid frequency owing to the existence of physical squint angle  $\theta_{\text{sq}}$ ,  $B_d$  is the bandwidth of the transmitted chirp signal,  $B_a \cos\theta_{\text{sq}}$  is equal to  $2v \cos\theta_{\text{sq}}/D$ , which corresponds to the Doppler bandwidth of the stripmap mode in the squint case, the presence of  $\cos\theta_{\text{sq}}$  is due to the squint angle  $\theta_{\text{sq}}$ , the factor  $(1 + (T_1/T_s))$  is because of the increase of the number of the received echoes backscattered by each target in the illuminated scene with respect to the strip mode,  $\varepsilon$  is the ratio of  $B_d$  to carrier frequency and can be expressed as  $\lambda B_d/c$ , and  $\mathbb{C}$  is a nonessential constant. To simplify the computation,  $r_0$  can be expressed as the range-invariant component and the range-variant component:  $r_0 = r + r_m$ , where  $r_m$  (the range-invariant component) is the midswath range and  $r$  (the range-variant component) describes the range variation around the midswath range:  $r \in [-\Delta r/2, \Delta r/2]$ ;  $\Delta r$  is the width of slant-range swath. By inserting  $r_0 = r + r_m$  into (11) and (12), we have

$$\Psi_a(f_a, f) = \chi_1(f_a, f) + \chi_2(f_a, f) \quad (14)$$

$$\chi_1(f_a, f) = \frac{f^2}{2K_r} + \frac{2r_m}{\lambda} \sqrt{\left(1 + \varepsilon \frac{f}{B_d}\right)^2 - \left(\frac{\lambda f_a}{2v}\right)^2} \quad (15)$$

$$\chi_2(f_a, f) = \frac{2r}{\lambda} \sqrt{\left(1 + \varepsilon \frac{f}{B_d}\right)^2 - \left(\frac{\lambda f_a}{2v}\right)^2} + f_a s_0. \quad (16)$$

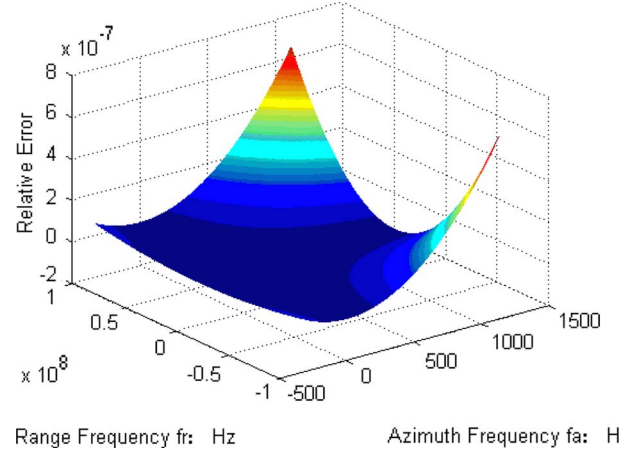


Fig. 2. Relative error from approximation. The maximum of relative error is  $6.7612 \times 10^{-007}$ ,  $f_{\text{Dc}} = 400$  Hz, and  $\theta_{\text{sq}} = 2.2^\circ$ .

Accordingly, (10) can be rewritten as follows:

$$\begin{aligned} \overline{H}_{\text{spot}}(f_a, f) &= \mathbb{C} \text{rect}\left[\frac{f_a - f_{\text{Dc}}}{(1 + T_1/T_s)B_a \cos\theta_{\text{sq}}}\right] \text{rect}\left[\frac{f}{B_d}\right] \\ &\quad \times \text{RF}_0 \iint_{\Sigma} \sigma(s_0, r_0) \exp[-j2\pi\chi_2(f_a, f)] \\ &\quad \times \text{rect}\left[\frac{s_0}{T_s}\right] ds_0 dr \end{aligned} \quad (17)$$

with

$$\text{RF}_0 = \exp[-j2\pi\chi_1(f_a, f)] \quad (18)$$

where  $\mathbb{C}_1 = \mathbb{C} \sqrt{r + r_m} \approx \mathbb{C} \sqrt{r_m}$ . To facilitate the FFT, (17) requires further approximation, which makes  $\chi_2(f_a, f)$  linearly dependent on  $f$ . Because  $\varepsilon \ll 1$  is almost always valid, (16) can be expanded as follows:

$$\chi_2(f_a, f) \approx [\alpha + \beta f_r]r + f_a s_0 \quad (19)$$

where

$$\beta = \frac{1}{\sqrt{1 - (\lambda f_a / 2v)^2}} \quad (20)$$

$$\alpha = \frac{2\sqrt{1 - (\lambda f_a / 2v)^2}}{\lambda}. \quad (21)$$

In (19),  $f_r = 2f/c$  is the range frequency variable. In order to show the precision of approximation, Fig. 2 shows the relative approximation error, which is given by  $[(\chi_2 - f_a s_0) - (\alpha + \beta f_r)r] / (\chi_2 - f_a s_0)$ . The maximum of the relative error, which is  $6.7612 \times 10^{-007}$ , shows that the precision of the model can meet the demands of processing algorithms with Doppler-centroid frequencies of 400 Hz. Substituting (19) into (17), we can obtain

$$\overline{H}_{\text{spot}}(f_a, f) = \text{RF}_1 \cdot \mathbb{Q}[f_a, \alpha + \beta f_r] \quad (22)$$

<sup>1</sup>When the bandwidth of transmitted signal is less than 10% of the carrier frequency, we consider that  $\varepsilon \ll 1$  holds.

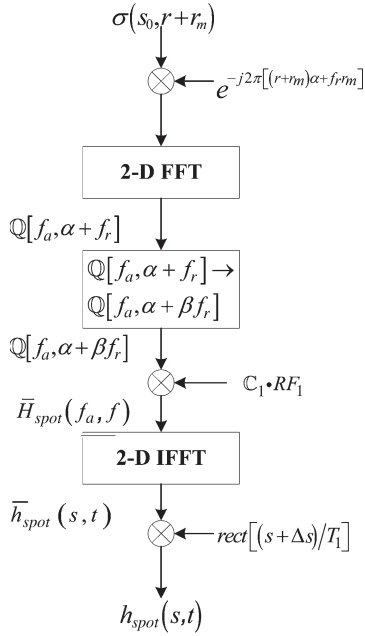


Fig. 3. Block diagram of spotlight raw signal simulator.

where

$$\begin{aligned} \text{RF}_1 = & \mathbb{C} \cdot \text{rect} \left[ \frac{f_a - f_{\text{Dc}}}{(1 + T_1/T_s) B_a \cos \theta_{\text{sq}}} \right] \text{rect} \left[ \frac{f}{B_d} \right] \\ & \times \text{RF}_0 \cdot \exp [j2\pi(\alpha + \beta f_r)r_m] \end{aligned} \quad (23)$$

$$\begin{aligned} \mathbb{Q}[f_a, f_r] = & \iint \sigma(s_0, r + r_m) \\ & \times \exp [-j2\pi(f_a s_0 + f_r(r + r_m))] ds_0 dr. \end{aligned} \quad (24)$$

In view of (20),  $\alpha + \beta f_r$  in (22) displays the essential characteristic of SAR: the coupling relation between the range and azimuth in the 2-D frequency domain. This nonlinear scaled term depends on both the range and azimuth frequencies and characterizes the range-dependent migration in the 2-D frequency domain.

From (7), (8), and (22), the spotlight SAR raw signal of the distributed target scene can be simulated according to the block diagram in Fig. 3.

The five steps in Fig. 3 are employed to obtain the squint spotlight raw signal. The advantage of the procedure is obvious: Only FFT operations and complex multiplication are needed, thus dramatically reducing the computational load with respect to the time-domain simulation method [5].

We employ  $(1 + (T_1/T_s)) \cdot \text{PRF}$  as the azimuth sample frequency in generating  $\sigma(s_0, r + r_m)$ , which will avoid azimuth aliasing. At last, in raw signal domain, a down-sampling operation is needed to recover the raw signal corresponding to the actual pulse repetition frequency (PRF).

It is evident that the emphasis of the procedure is on how to implement  $\mathbb{Q}[f_a, \alpha + f_r] \rightarrow \mathbb{Q}[f_a, \alpha + \beta f_r]$ , which is located in the third step of Fig. 3. We can see that  $\mathbb{Q}[f_a, \alpha + \beta f_r]$  is located in the new coordinate  $[f_a, \alpha + \beta f_r]$ , instead of the conventional one  $[f_a, f_r]$ . The additional, nonlinear, and scaled

term  $\beta$  depends on the azimuth frequency and characterizes the range migration, which is often referred to as Stolt mapping [10] or grid deformation [11]. Owing to the fact that SAR raw signals are digital signals, step 3 can require a perfect complex interpolation. However, as we know, perfect interpolation requires an infinite length of kernel and is badly time-consuming. In practice, some may make a compromise between no interpolation and perfect interpolation with a four- or eight-point interpolator. However, it is also relatively costly. Therefore, the perfect and efficient implementation  $\mathbb{Q}[f_a, \alpha + f_r] \rightarrow \mathbb{Q}[f_a, \alpha + \beta f_r]$  is crucial to spotlight raw signal simulation. In this paper, we employ some simple optical systems to show analog signal processing methods that only involve complex multiplications and FFTs. These signal systems will be discussed particularly in the next section.

### III. APPLICATION OF OPTICAL THEORIES IN COUPLING THE RANGE AND AZIMUTH

The earliest imaging systems were optical imaging systems, and they are still the most common imaging systems. In the following, we first explain some important optical theories.

According to the Huygens–Fresnel principle, if a monochromatic wave  $g(x, y, z)$  takes the value  $g_0(x, y)$  in the  $x, y$  plane at  $z = 0$ , then in the  $x, y$  plane at  $z = d$ , it takes the value [12]–[14]

$$g_d(x, y) = h(x, y) \otimes g_0(x, y) \quad (25)$$

where  $\otimes$  expresses the 2-D convolution operator;  $h(x, y)$  is the Huygens–Fresnel point spread function of free space and can be described with Fresnel approximation as follows:

$$h(x, y) = \exp \left\{ j \frac{\pi}{\lambda d} (x^2 + y^2) \right\} \quad (26)$$

where  $\lambda$  is the wavelength. Therefore, monochromatic wave propagation corresponds to convolving with a chirp signal.

As for a thin lens (ideal lens), it suffices to determine the change in the incident wave as it passes through it. If the field in the  $x, y, z = 0^-$  plane (to the left of the lens), then, it can be shown that  $z = 0^+$  plane. It is given by the product [12]–[14]

$$g_{d0+}(x, y) = g_{d0-}(x, y) \exp \left\{ -j2\pi \frac{(x^2 + y^2)}{\lambda f_l} \right\} \quad (27)$$

where  $f_l$  is the focal length of the lens. Hence, thin lens can introduce a quadratic phase factor.

A lens can perform either of two processing tasks: an image or a 2-D dimensional Fourier transform [13]. In the following, we will discuss some processing methods to complete the coupling relation between the range and azimuth with the two abilities previously presented. For simplicity, we describe the coupling relation between the range and azimuth for each  $f_a$  frequency as follows:

$$\mathbb{Q}[f_r] \rightarrow \mathbb{Q}[\beta f_r]. \quad (28)$$

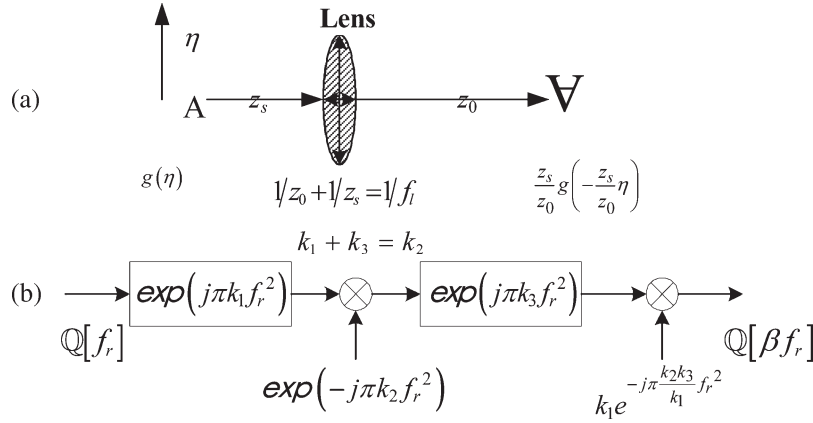


Fig. 4. (a) Optical system that can form a magnified imager. (b) Corresponding signal processing system that can obtain the desirable result.

#### A. Couple the Range and Azimuth With Lens as an Imager

The transformation shown in (28) is the analog equivalent to magnification in an optical system with a lens as an imager, shown in Fig. 4. Fig. 4(a) shows an optical system that is simplified as a 1-D system. Suppose the object  $g(\eta)$  located at a distance  $z_s$  from a lens of focal length  $f_l$ . Here,  $\eta$  represents the vertical spatial coordinate.

If we define the output plane to be at distance  $z_0$  from the lens and select  $z_0$  such that it satisfies the lens formula  $1/z_0 + 1/z_s = 1/f_l$ , which is corresponding to  $k_1 + k_3 = k_2$  of the signal processing system shown in Fig. 4(b), the output object is reversed and magnified by a factor  $z_0/z_s$ , which is a desirable scale factor. Using the processing block diagram shown in Fig. 4(b), we can produce a transformation method to perform scale transform at arbitrary ratio. Let us now consider the coefficients shown in Fig. 4(b) wherein the coefficients  $k_1$ ,  $k_2$ , and  $k_3$  must satisfy the following [14]:

$$\begin{cases} k_1 + k_3 = k_2 \\ -k_3/k_1 = \beta. \end{cases} \quad (29)$$

The signal processing system can be described in the following:

$$\mathcal{Q}[\beta f_r] = \left\{ \left( \mathcal{Q}[f_r] * e^{j\pi k_1 f_r^2} \right) \cdot e^{-j\pi k_2 f_r^2} \right\} * k_1 e^{-j\pi \frac{k_2 k_3}{k_1} f_r^2} \quad (30)$$

where  $*$  expresses the 1-D convolution operator. Different selections of the three coefficients in the no-define state are possible with some limitations, which are discussed in detail in [15]. When satisfying a given term, it can be seen as inverse chirp scaling algorithm.

#### B. Couple the Range and Azimuth With Lens as a Fourier Transformer

When an object is located in a plane at  $z_s = f_l$ , the thin lens can also be used to perform another useful function, which is the Fourier transform. Therefore, we consider that both the input and output planes are located in a focal distance from the lens [13], [14], shown in Fig. 5(a) (the nonessential amplitude factor is neglected).

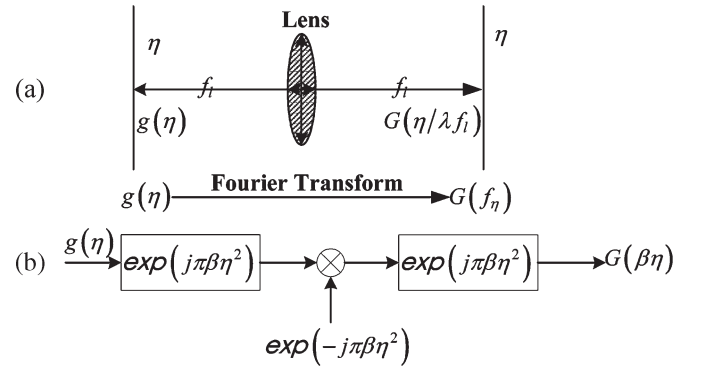


Fig. 5. (a) Optical Fourier transform system. (b) Corresponding signal processing system that produces a similar result.  $f_\eta$  is the frequency variable with respect to the variable  $\eta$ .  $G(f_\eta)$  is the Fourier transform of  $g(\eta)$ .

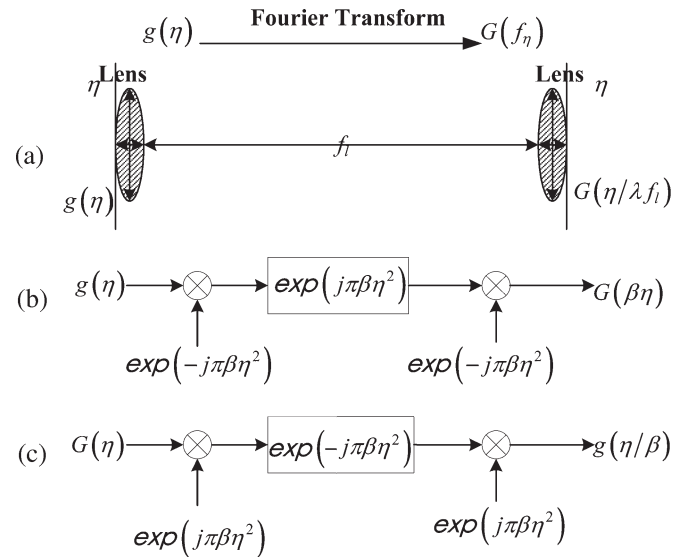


Fig. 6. (a) Optical Fourier transform system of dual lens. (b) Corresponding signal processing system that produces scaled Fourier transform. (c) Corresponding signal processing system that produces inverse scaled Fourier transform.

In the system shown in Fig. 5, the scaled Fourier transform of input signal is obtained in the output plane. Based on the preceding system, we consider the following optical system

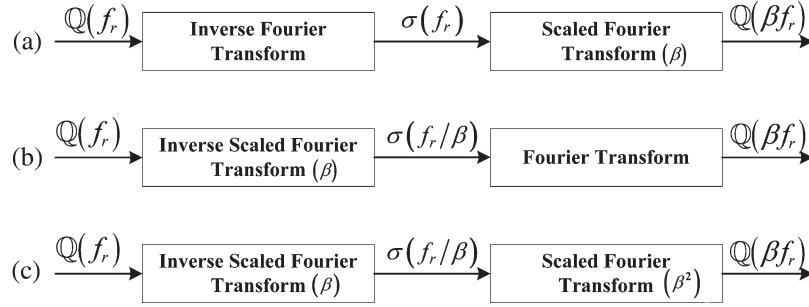


Fig. 7. (a) Weave of inverse Fourier transform and scaled Fourier transform. (b) Weave of inverse scaled Fourier transform and Fourier transform. (c) Weave of inverse scaled Fourier transform and scaled Fourier transform.

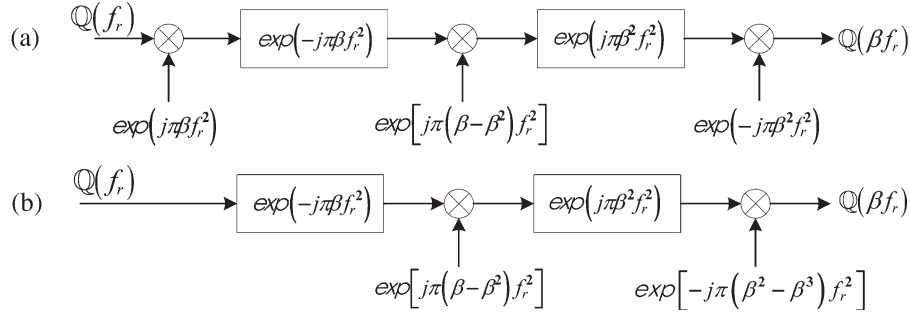


Fig. 8. (a) Signal processing block obtained from Fig. 6(c). (b) Alternative implementation of the procedure in Fig. 7(a).

with dual lenses, shown in Fig. 6(a). Using the systems shown in Figs. 5(b) and 6(b), we can easily produce the scaled Fourier transform, which is defined in [16] and also called as chirp Fourier transformation in [17]. Fig. 6(c) shows an analog inverse scaled Fourier transform. In view of Figs. 5(b) and 6(b) and (c), the scaled Fourier transform and inverse scaled Fourier transform are described in the following, wherein  $*$  expresses the 1-D convolution

$$G(\beta\eta) = \left( [g(\eta) \cdot e^{-j\pi\beta\eta^2}] * e^{j\pi\beta\eta^2} \right) \cdot e^{-j\pi\beta\eta^2} \quad (31)$$

$$g(\eta/\beta) = \left( [G(\eta) \cdot e^{j\pi\beta\eta^2}] * e^{-j\pi\beta\eta^2} \right) \cdot e^{j\pi\beta\eta^2}. \quad (32)$$

However, owing to the fact that the input and output of the transform systems shown in Figs. 5(b) and 6(b) and (c) are put into the two different domains instead of our desirable scaled transform in the same frequency domain, we need to employ some ways to combine forward and inverse Fourier transform and scaled Fourier transform to complete the desirable scaled transform in the frequency domain. These assembled systems are shown in Fig. 7. In Fig. 7(a), an inverse Fourier transform and scaled Fourier transform, whose scaling factor is  $\beta$ , are combined to obtain the desirable scaling result. In Fig. 7(b), the inverse scaled Fourier transform, the scaling factor of which is also  $\beta$ , and the Fourier transform are combined. The block diagram of Fig. 7(c) shows the inverse scaled Fourier transform and scaled Fourier transform, whose scaling factors are  $\beta$  and  $\beta^2$ , respectively.

TABLE I  
SPOTLIGHT SYSTEM DATA USED IN THE SIMULATION RESULTS

Platform Velocity ( $v$ )	160m/s
Wavelength ( $\lambda$ )	0.03125m
Pulse duration ( $\tau$ )	20.4us
Bandwidth ( $B_r$ )	110MHz
Pulse repetition frequency (PRF)	1400Hz
Squint angle ( $\theta_{sq}$ )	2.2°
Mid-swath range ( $r_m$ )	5500m
Spotlight mode gain ( $T_l/T_s$ )	3

The system shown in Fig. 7(c) is a special case of one shown in Fig. 4(b). To show the relation between them, the system in Fig. 7(c) is described further in Fig. 8.

In Fig. 8(a), the first term in the left can be shifted to the right and combined with the last term based on the linear system theory, which is shown in Fig. 8(b). Comparing the two systems shown in Figs. 4(b) and 8(b), it can be seen that the two systems are equivalent if only the parameters  $k_1$ ,  $k_2$ , and  $k_3$  satisfy the following:

$$\begin{cases} k_1 = -\beta \\ k_2 = \beta^2 - \beta \\ k_3 = \beta^2. \end{cases} \quad (33)$$

In particular, one complex multiplication can be saved in the system shown in Fig. 8(b) compared with the one shown in Fig. 8(a).

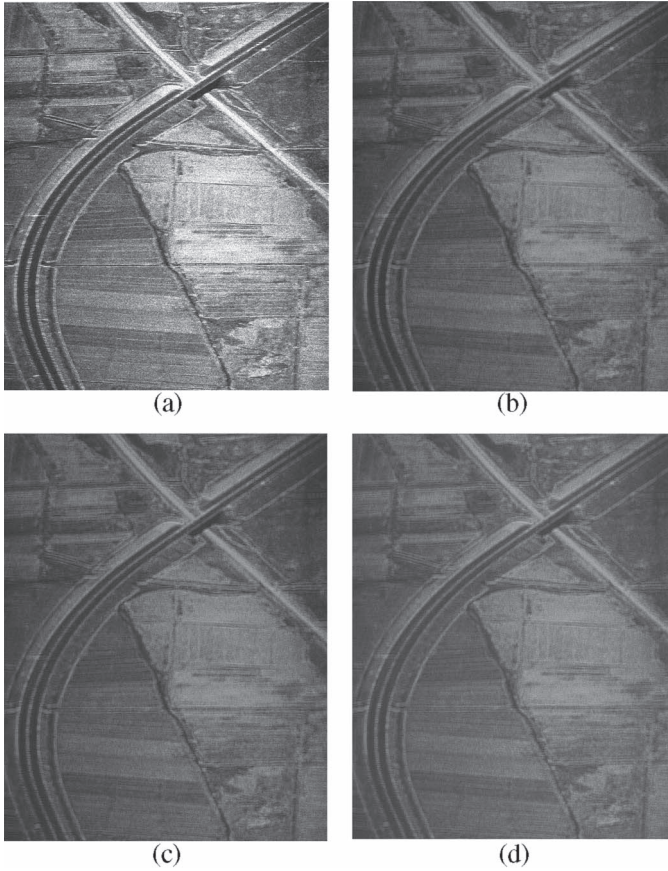


Fig. 9. (a) Scattering coefficient matrix of the scene. (b) Result of simulation methods shown in Figs. 4(b) and 7(c). (c) Result of the simulation method shown in Fig. 7(a). (d) Result of simulation method shown in Fig. 7(b).

From previous discussions, it is clear that the methods derived from simple optical principles are carried out only by complex multiplication and FFT. The scaling operations, which are shown in Figs. 4 and 7, are independent of the transmitted signal, which means that the transmitted signal is not limited to chirp signal.

#### IV. SIMULATION RESULT AND ANALYSIS OF PERFORMANCE

##### A. Simulation Result

In this section, we carry out the simulation to validate the proposed simulation approach. The main parameters are listed in Table I.

In this simulation, we use a focused spotlight SAR image, the size of which is  $2048 \times 1024$  pixels, as a scattering coefficient matrix, i.e.,  $\sigma(s_0, r + r_m)$ , as shown in Fig. 9(a). By using the scattering coefficient matrix, the processing procedure shown in Fig. 3 is used to generate the spotlight SAR raw data. The transformation  $\mathbb{Q}[f_a, \alpha + f_r] \rightarrow \mathbb{Q}[f_a, \alpha + \beta f_r]$  is replaced with the block diagram shown in Figs. 4(b) and 7(a) and (b), respectively.

Using the aforementioned processing procedure, the range and azimuth coupling phase information is involved in the generated raw data. To validate the phase information of the raw data, a standard focusing algorithm [7] is used to process the

simulated data. The focused results are shown in Fig. 9(b)–(d). Comparing the original scattering coefficient matrix shown in Fig. 9(a) and the focused images of the simulated raw data shown in Fig. 9(b)–(d), we can know that our method is right.

##### B. Performance Analysis

In the algorithms previously described, the main operations are the complex multiplications and additions. Owing to the fact that complex multiplications consume much more time and resources of the computer than complex additions, we employ the complex multiplications to indicate the computational complexity of the described algorithms. The consumed complex multiplications from steps 1 to 2 in Fig. 3 can be expressed as follows [5]:

$$N_{\text{FD}} \approx N_a N_r g [1 + \log_2(N_a N_r) + \log_2 g] \quad (34)$$

where  $N_{\text{FD}}$  is the number of complex multiplications;  $N_a$  and  $N_r$  are the pixels in the azimuth and range dimensions, respectively;  $g = 1 + (T_1/T_s)$  usually ranges from two to five. The consumed complex multiplications from the operation shown in Figs. 4(b) and 7(c) are expressed as follows:

$$N_{\text{offset}} = 4N_a N_r [1 + \log_2 N_r/2]. \quad (35)$$

Moreover, the consumed complex multiplications corresponding to Fig. 7(a) and (b) can be expressed as follows:

$$N_{\text{offset}} = 3N_a N_r [1 + \log_2 N_r/2]. \quad (36)$$

The last three steps need complex multiplications  $N_{\text{de}} = 2N_r N_a + (N_r N_a/2)[\log_2 N_r + \log_2 N_a]$ . Therefore,  $N_{\text{FD}} + N_{\text{offset}} + N_{\text{de}}$  complex multiplications are required, according to the proposed algorithms.

If the spotlight raw signal is directly evaluated in the time domain, the computational complexity is as follows [5]:

$$N_{\text{TD}} \approx (N_a N_r)^2 \quad (37)$$

where  $N_{\text{TD}}$  is the number of complex multiplications in the time-domain simulation. Accordingly, by using the frequency-domain method, the processing time can be reduced by a factor

$$\frac{N_{\text{TD}}}{N_{\text{FD}} + N_{\text{offset}} + N_{\text{de}}} \approx \frac{N_a N_r}{(g + 0.5) \log_2(N_a N_r)}. \quad (38)$$

For a  $2048 \times 1024$  distributed target scene, if given  $g = 4$ , the decrease factor of processing time is 4236, which shows that the frequency-domain method is more efficient.

#### V. CONCLUSION

In this paper, a squint spotlight model in the 2-D frequency domain has been derived. According to the model, several frequency-domain methods have been developed to simulate the spotlight raw signal. To show the coupling relation between the range and azimuth in the 2-D frequency domain, we have

used some tricks from optical principles to complete the scaling transform. From the analysis, it can be seen that the simulation method is efficient, owing to the fact that only complex multiplications and FFTs are needed.

The presented simulation method can be applied in the real-time raw signal simulator. For its efficiency, the output data of the simulator can be directly used as the input signal of the real-time processor, which can efficiently verify and test the performance of the processor.

#### ACKNOWLEDGMENT

The authors would like to thank the anonymous reviewers for their very constructive and encouraging criticism, helping to improve the final paper.

#### REFERENCES

- [1] G. Franceschetti and R. Lanari, *Synthetic Aperture Radar Processing*. Boca Raton, FL: CRC, 1999.
- [2] G. Franceschetti, M. Migliaccio, D. Riccio, and G. Schirinzi, "SARAS: A SAR raw signal simulator," *IEEE Trans. Geosci. Remote Sens.*, vol. 30, no. 1, pp. 110–123, Jan. 1992.
- [3] G. Franceschetti, M. Migliaccio, and D. Riccio, "SAR simulation of actual ground sites described in terms of sparse input data," *IEEE Trans. Geosci. Remote Sens.*, vol. 32, no. 6, pp. 1160–1169, Nov. 1994.
- [4] G. Franceschetti, A. Iodice, M. Migliaccio, and D. Riccio, "A novel across-track SAR interferometry simulator," *IEEE Trans. Geosci. Remote Sens.*, vol. 36, no. 3, pp. 950–962, May 1998.
- [5] S. Cimmino, G. Franceschetti, A. Iodice, D. Riccio, and G. Ruello, "Efficient spotlight SAR raw signal simulation of extended scenes," *IEEE Trans. Geosci. Remote Sens.*, vol. 41, no. 10, pp. 2329–2337, Oct. 2003.
- [6] G. Franceschetti, A. Iodice, S. Perna, and D. Riccio, "SAR sensor trajectory deviations: Fourier domain formulation and extended scene simulation of raw signal," *IEEE Trans. Geosci. Remote Sens.*, vol. 44, no. 10, pp. 2323–2334, Sep. 2006.
- [7] J. Mittermayer, A. Moreira, and O. Loffeld, "Spotlight SAR data processing using the frequency scaling algorithm," *IEEE Trans. Geosci. Remote Sens.*, vol. 37, no. 5, pp. 2198–2214, Sep. 1999.
- [8] R. K. Raney, H. Runge, R. Bamler, I. G. Cumming, and F. H. Wong, "Precision SAR processing using chirp scaling," *IEEE Trans. Geosci. Remote Sens.*, vol. 32, no. 4, pp. 786–799, Jul. 1994.
- [9] W. G. Carrara, R. S. Goodman, and R. M. Majewski, *Spotlight Synthetic Aperture Radar: Signal Processing Algorithms*. Norwood, MA: Artech House, 1995.
- [10] R. H. Stolt, "Migration by Fourier transform techniques," *Geophysics*, vol. 43, no. 1, pp. 49–76, 1978.
- [11] G. Franceschetti, R. Lanari, V. Pascasio, and G. Schirinzi, "WASAR: A wide-angle SAR processor," *Proc. Inst. Electr. Eng.—Radar Sonar Navig.*, vol. 139, no. 2, pp. 107–114, Apr. 1992.
- [12] J. W. Goodman, *Introduction to Fourier Optics*. New York: McGraw-Hill, 1968.
- [13] R. E. Blahut, *Theory of Remote Image Formation*. Cambridge, U.K.: Cambridge Univ. Press, 2004.
- [14] A. Papoulis, *Systems and Transforms With Applications in Optics*. New York: McGraw-Hill, 1968.
- [15] M. Y. Jin, F. Cheng, and M. Chen, "Chirp scaling algorithms for SAR processing," in *Proc. IGARSS*, Tokyo, Japan, 1993, pp. 1169–1171.
- [16] O. Loffeld, F. Schneider, and A. Hein, "Focusing SAR images by inverse scaled Fourier transformation," in *Proc. Int. Conf. Signal Process. Commun.*, Canary Islands, Spain, Feb. 1998, pp. 537–540.
- [17] D. C. Munson and O. Arhan, "Interpolation and the chirp transform: DSP meets optics," in *Proc. ICASSP*, Phoenix, AZ, Mar. 1999, pp. 2099–2102.



**Yu Wang** (M'07) received the B.S. degree in control engineering from the University of Henan, Kaifeng, China, in 2002 and the Dr.Eng. degree from the Graduate University of the Chinese Academy of Sciences, Beijing, China, in 2007.

His research interests include monostatic and bistatic SAR signal processing, bistatic interferometric, airborne SAR motion compensation, SAR raw signal simulation, optimization theory, and adaptive signal processing.



**Zhimin Zhang** received the B.S. degree in electrical engineering from the Beijing Institute of Technology, Beijing, China, in 1992 and the M.S. degree from the Graduate University of Chinese Academy of Sciences, Beijing, in 1995.

Since 1995, he has been with the Institute of Electronics, Chinese Academy of Sciences, where he has been working on radar system design and signal processing. His research interests include spaceborne/airborne SAR technology for advanced modes, real-time signal processing, and multifunctional radar imaging.



**Yunkai Deng** received the M.S. degree in electrical engineering from the Beijing Institute of Technology, Beijing, China, in 1993.

He has been with the Institute of Electronics, Chinese Academy of Sciences (IECAS), Beijing, since 1993, where he has been working on antenna design, microwave circuit design, and spaceborne/airborne SAR technology. He has been the Leader of several spaceborne/airborne SAR projects and developed some key technologies of spaceborne/airborne SAR. Currently, he is a Research Scientist, a

member of the scientific board, and the Director of the Spaceborne Microwave Remote Sensing Department, IECAS. His current research interests include spaceborne/airborne SAR technology for advanced modes, multifunctional radar imaging, and microwave circuit design.